Supporting Information

Synchronous Repair of Intrinsic Thermal Conductivity and Mechanical Performance of Aramid Nanofiber Films through Hydrogen-Bonding Reconstruction

Niu Jiang, Yu-Yang Song, Mei-Yan Pu, Hong Cao, Ya-Jun Fu, Lu Bai, Jie Yang, Wei Yang**

College of Polymer Science and Engineering, Sichuan University, State Key Laboratory of Advanced Polymer Materials, Chengdu 610065, Sichuan, P. R. China.

*Corresponding authors: psejieyang@scu.edu.cn (J. Yang); weiyang@scu.edu.cn (W. Yang); Fax: +86 28 8546 0130; Tel: +86 288546 0130

* Corresponding authors: psejieyang@scu.edu.cn (J. Yang), weiyang@scu.edu.cn (W. Yang).

1. Simulation of Phonon Density of States Using Molecular Dynamics

The phonon density is calculated by velocity auto-correlation function method in NVE ensemble. Prior to the formal MD simulations, pre-equilibration processes are conducted, beginning with MD runs of 4,000,000 timesteps under NPT ensemble at 300 K to relax the MD models, followed by MD simulations with 4,000,000 timesteps under NVT ensemble to further equilibrate the models. Finally, NEMD simulations are performed under NVE ensemble to achieve the temperature gradient. A small timestep of 0.25 fs is assigned in the MD simulations. The standard Newton's equations of motion in the polymer systems are integrated using the velocity-Verlet integration algorithm. The Polymer Consistent Force Field (PCFF) is utilized to describe the atomic interactions in both polymer systems.[S1] To describe the non-bonded interactions, the van der Waals (vdW) interactions are considered by the Lennard-Jones 9-6 potential with a cut-off distance of 15 Å, while the long-range electrostatic interactions are described by the standard Coulomb potential using the particle−particle−particle−mesh (PPPM) algorithm. All the classical MD simulations are performed at room temperature (300 K) using the LAMMPS.[S2]

2. Supplementary Figures

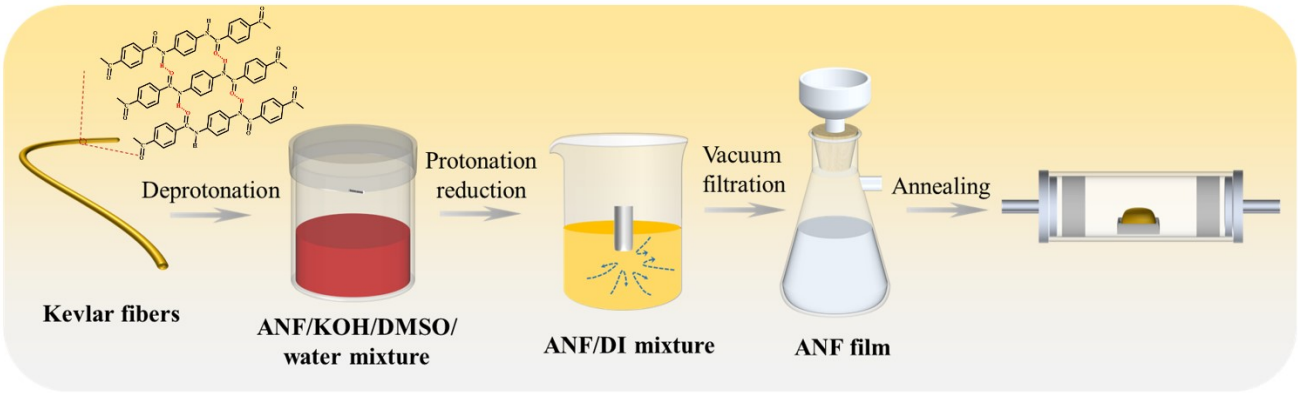

Fig. S1 Schematic of the fabrication process of ANF film.

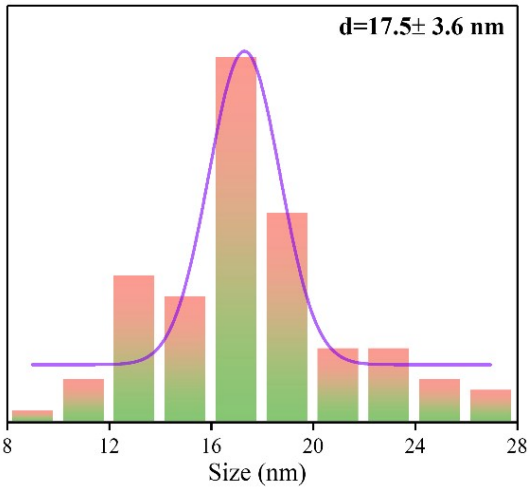

Fig. S2 Statistical analysis results of ANF based on TEM images.

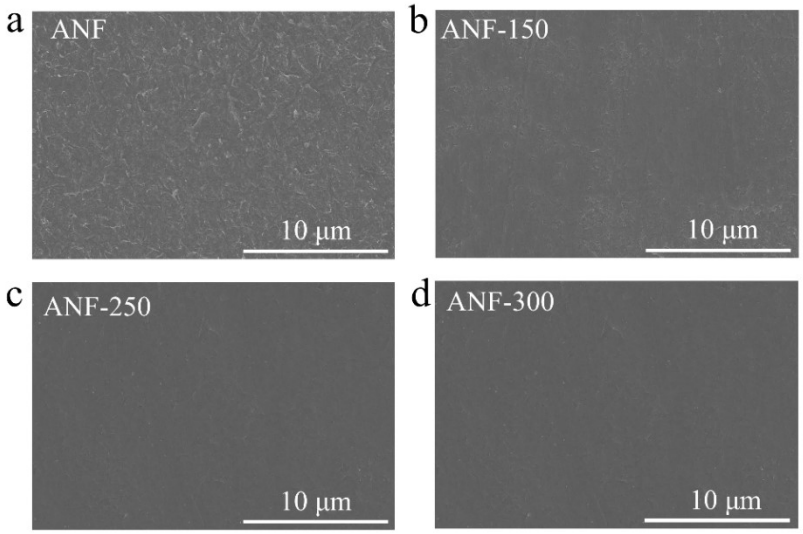

Fig. S3 SEM images of a) ANF, b ANF-150, c) ANF-250 and d) ANF-300 films.

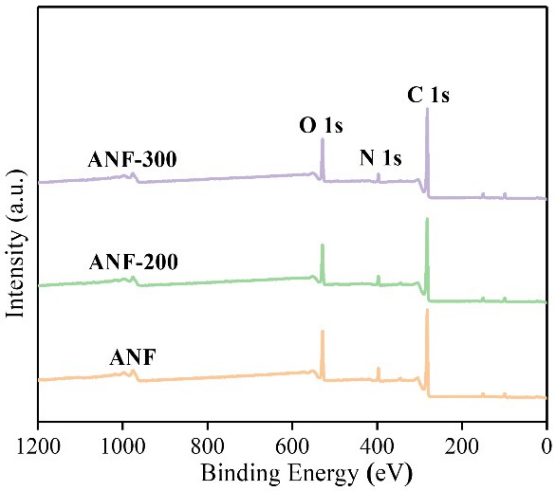

Fig. S4 XPS spectra of ANF films.

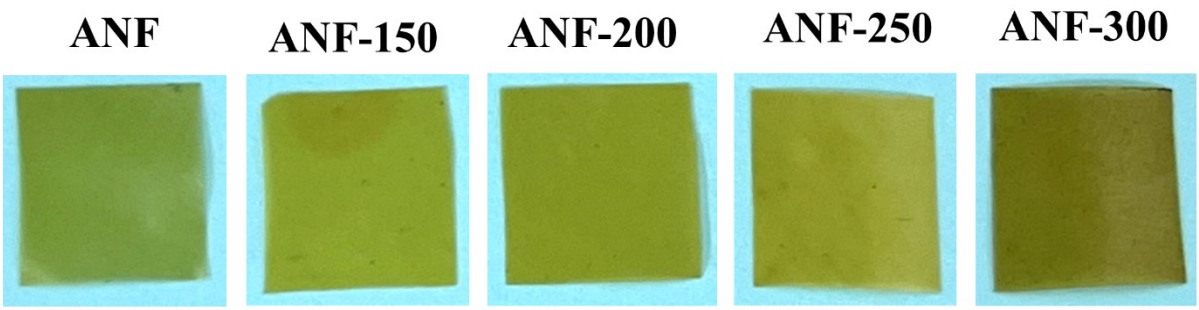

Fig. S5 Digital photographs capturing the thermochromic transition of ANF films.

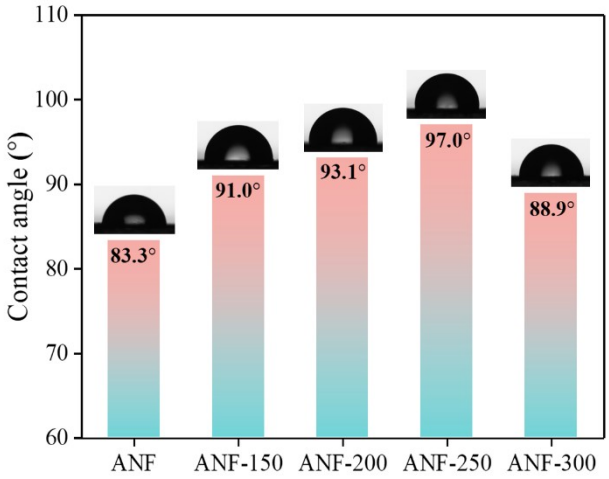

Fig. S6 Static water contact angle measurements assessing surface wettability with corresponding optical profilometry images of DI water droplets.

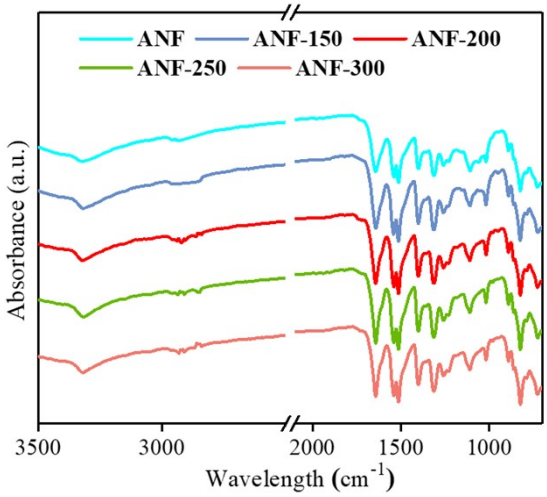

Fig. S7 Micro-FTIR spectra of ANF films.

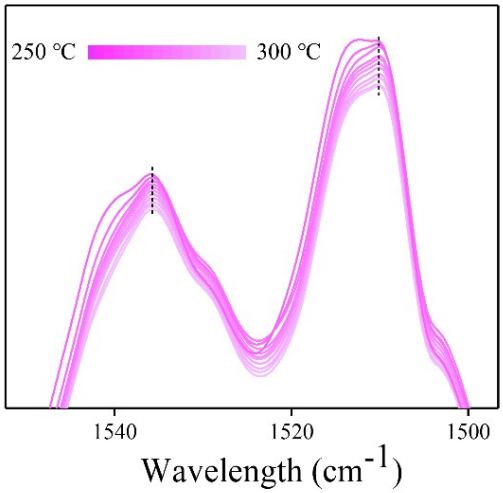

Fig. S8 *In-situ* FTIR spectra of ANF films recorded from 250 °C to 300 °C.

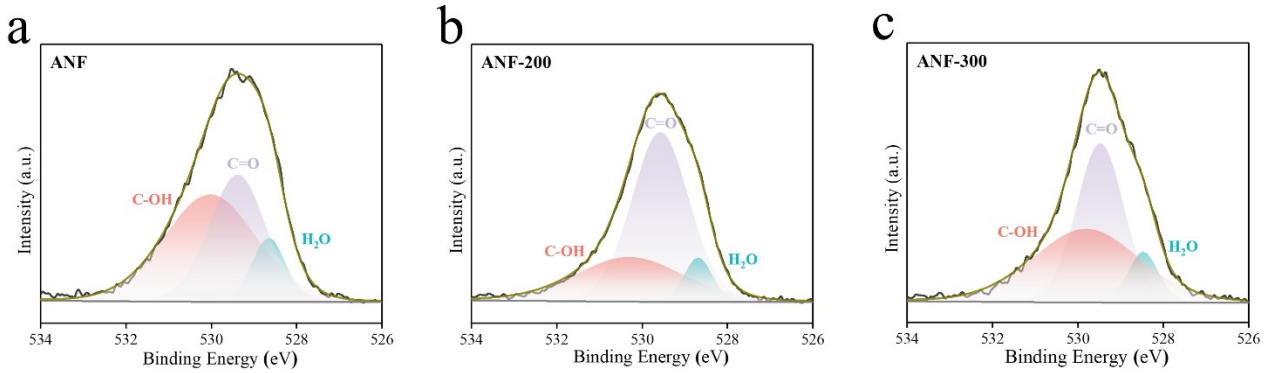

Fig. S9 High-resolution O 1s core-level XPS spectra of a) pristine ANF, b) ANF-200, and c) ANF-300 films.

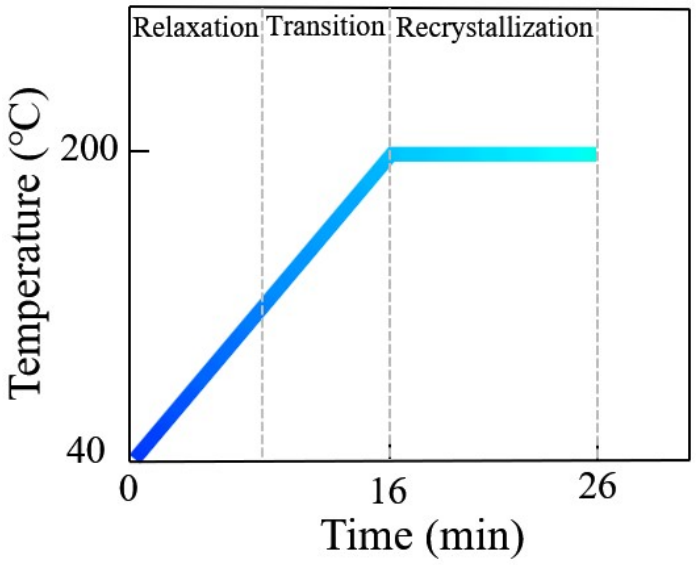

Fig. S10 Colors of the 1D WAXD curve corresponding to the variation of temperature over time.

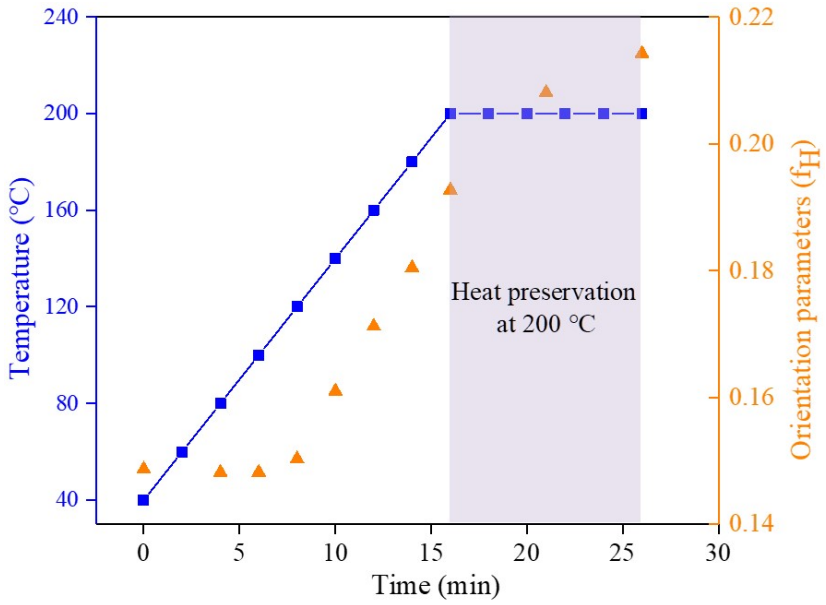

Fig. S11 Orientation parameter (f_H) of ANF films with the elevated temperatures.

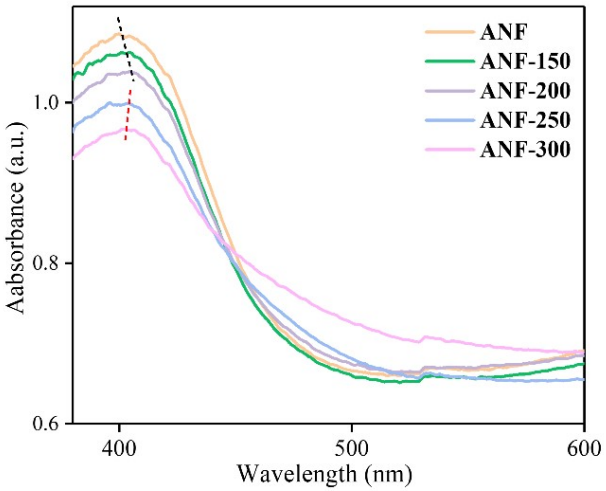

Fig. S12 UV-*vis*-NIR spectra of ANF films.

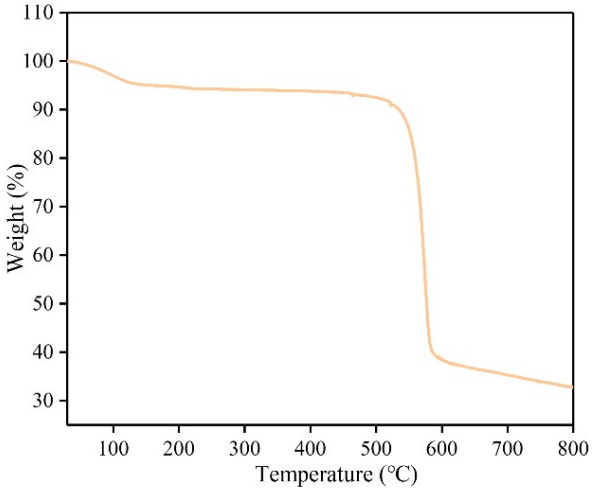

Fig. S13 TGA curves of Kevlar fibers.

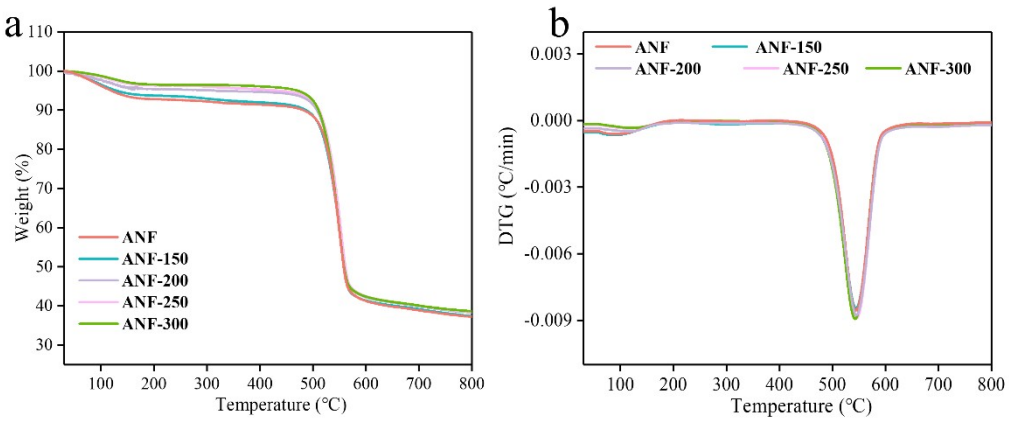

Fig. S14 (a) TGA and (b) DTG curves of ANF films.

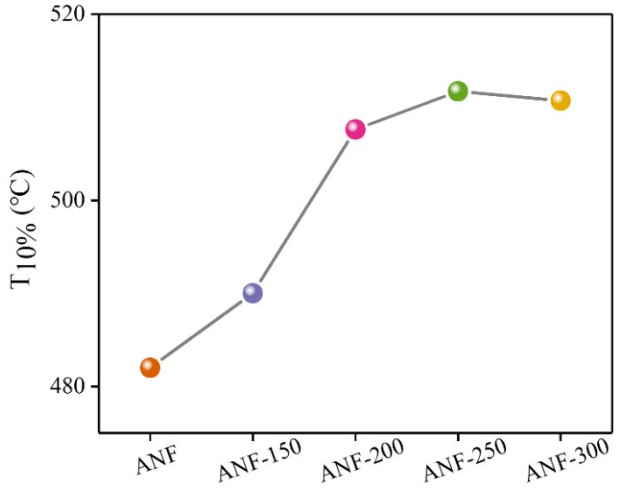

Fig. S15 Temperatures of ANF films at 10% weight loss based on TGA curves.

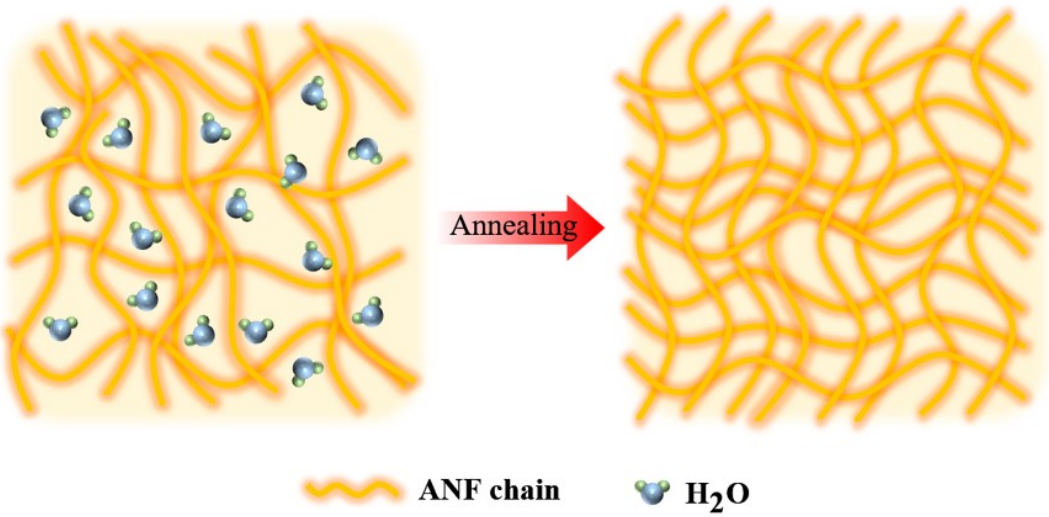

Fig. S16 Effect of binding water elimination on the molecular chain of ANF.

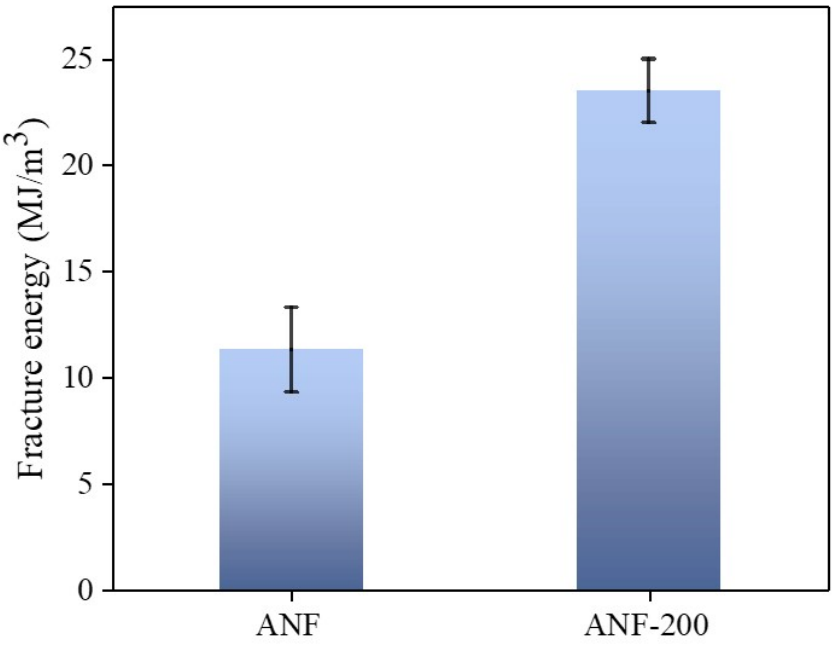

Fig. S17 Fracture energy of ANF and ANF-200 films.

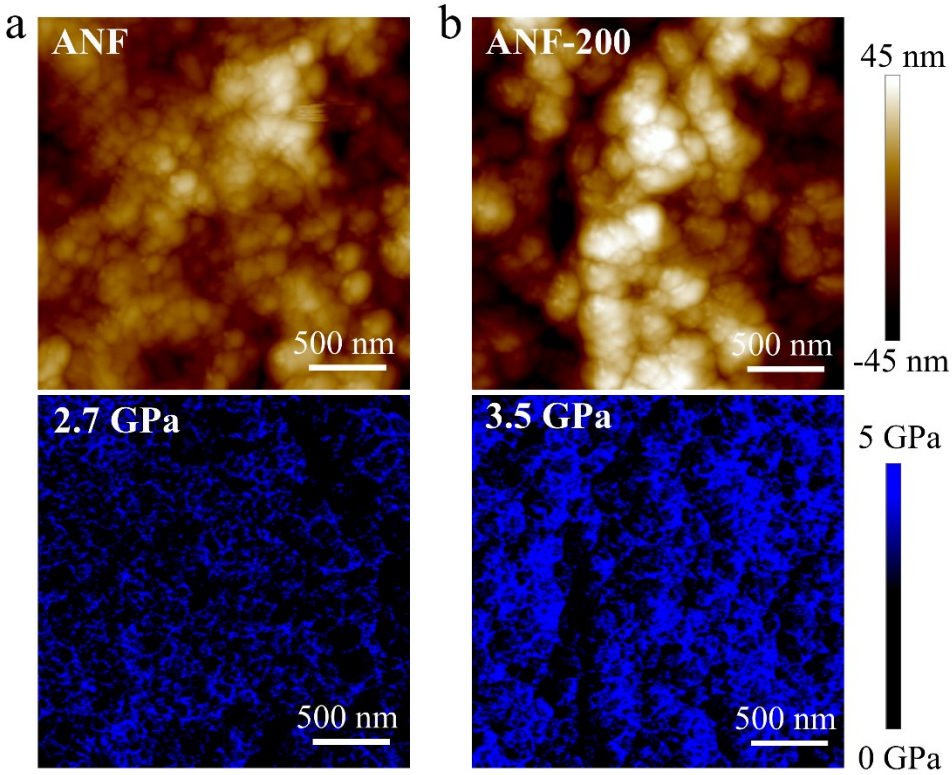

Fig. S18 AFM images showing the surface topography and the elastic modulus of a) ANF and b) ANF-200 films.

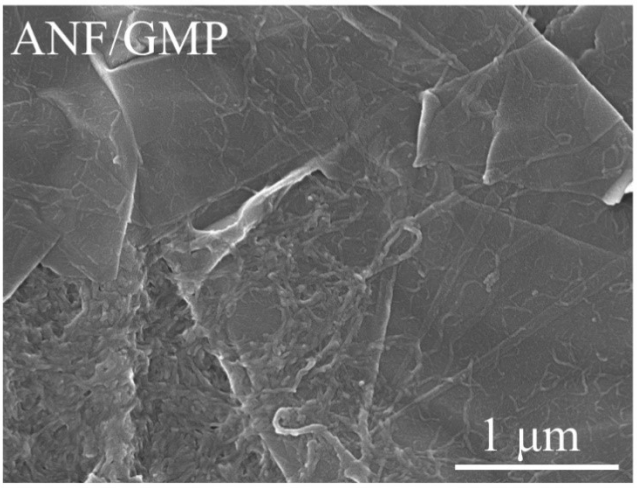

Fig. S19 Surface SEM image of ANF/GMP composite films.

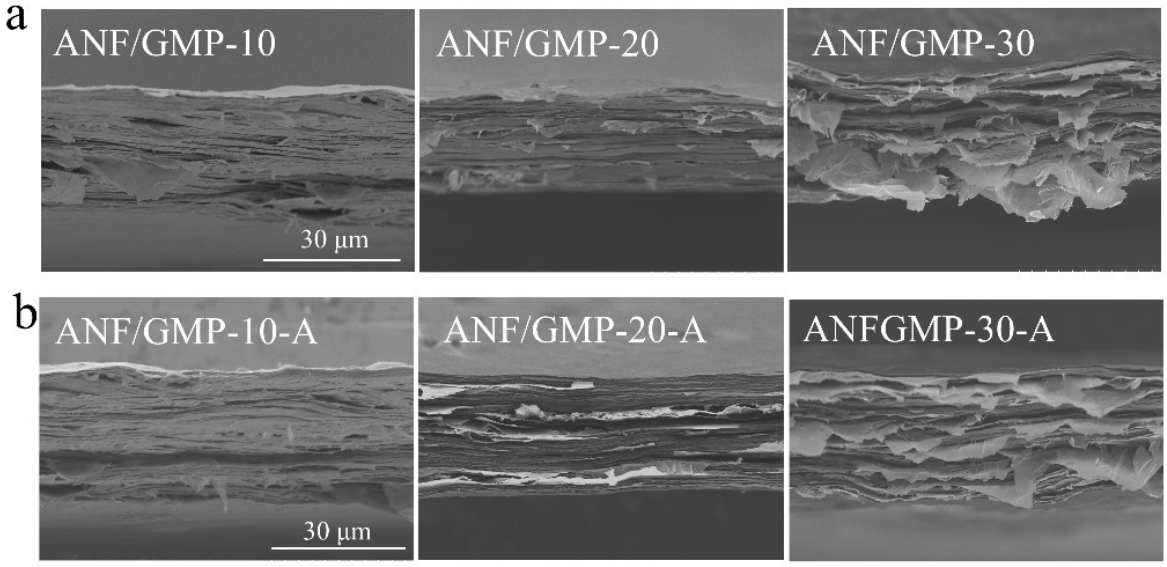

Fig. S20 Cross-sectional SEM images of a) ANF/GMP and b) ANF/GMP-A composite films.

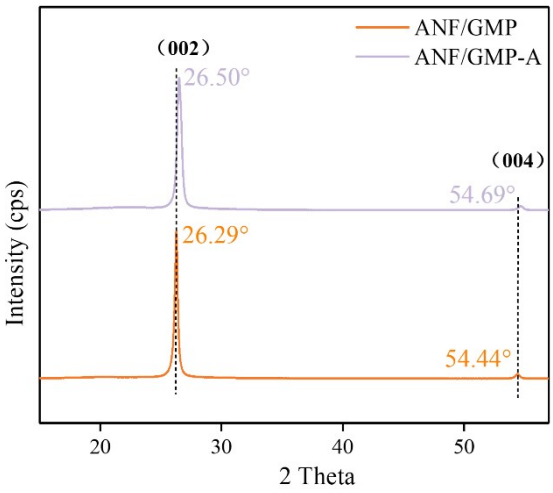

Fig. S21 XRD patterns of composite films.

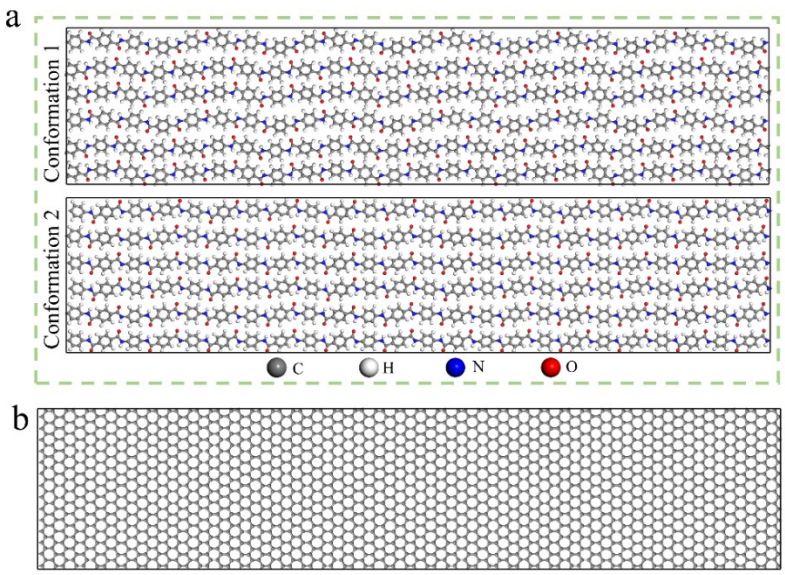

Fig. S22 Molecular models of the a) ANF with two conformations and b) GMP.

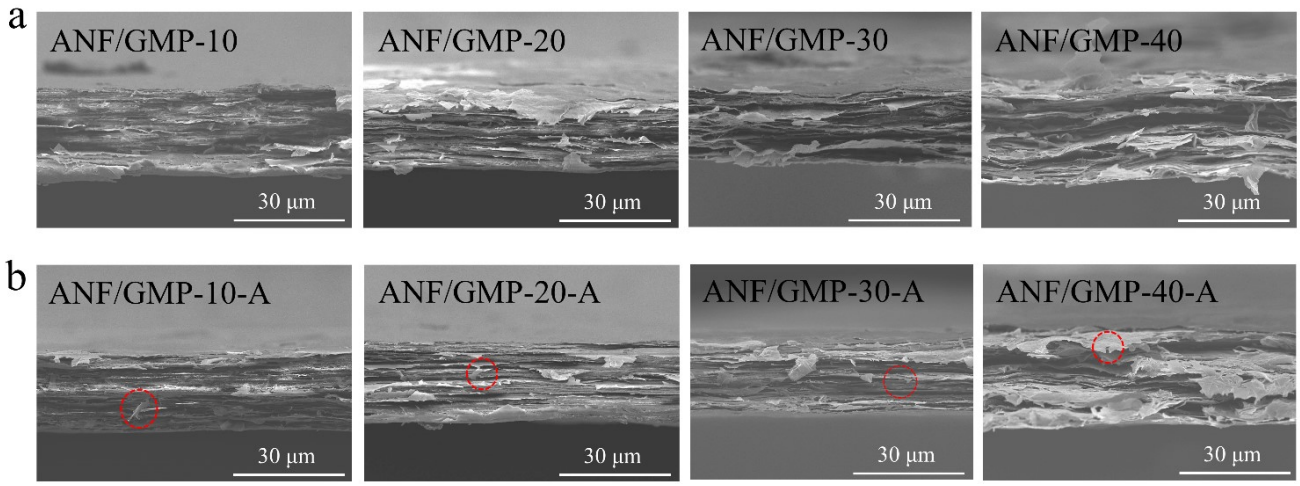

Fig. S23 Cross-sectional SEM images of ANF/GMP composite films after tensile measurements.

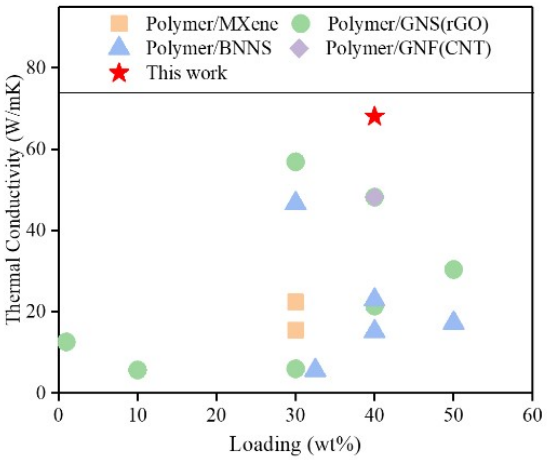

Fig. S24 Comparative analysis of the thermal conductivity of the ANF/GMP-40-A film with various nacre-like polymer-based thermally conductive composites (details are listed in Supplementary Table S3).

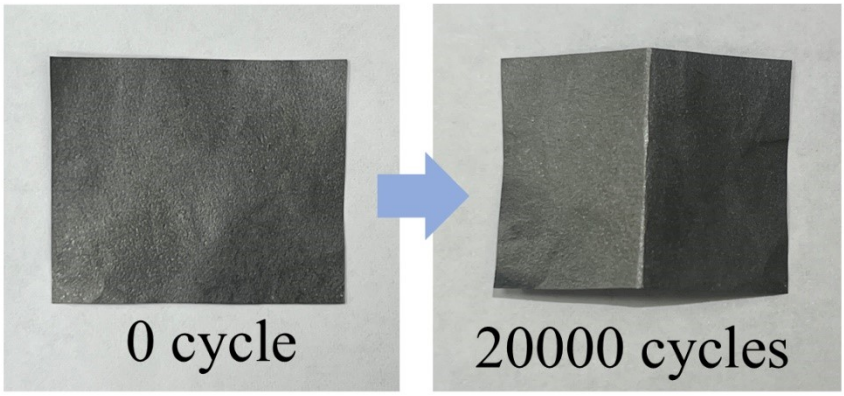

Fig. S25 Optical images demonstrating the bending resistance of the annealed composite film.

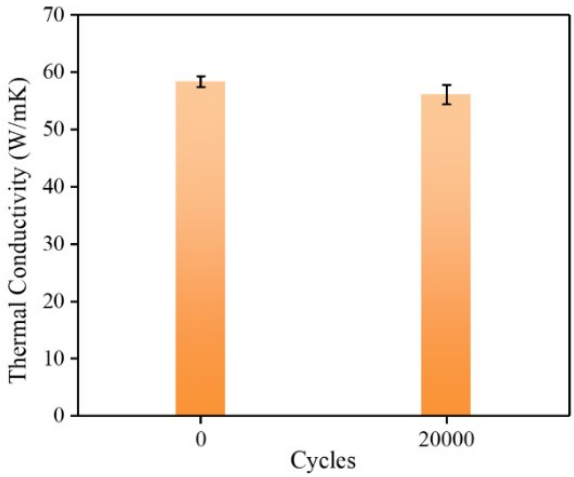

Fig. S26 Thermal conductivity variation of the annealed composite film after bending for 20000 cycles.

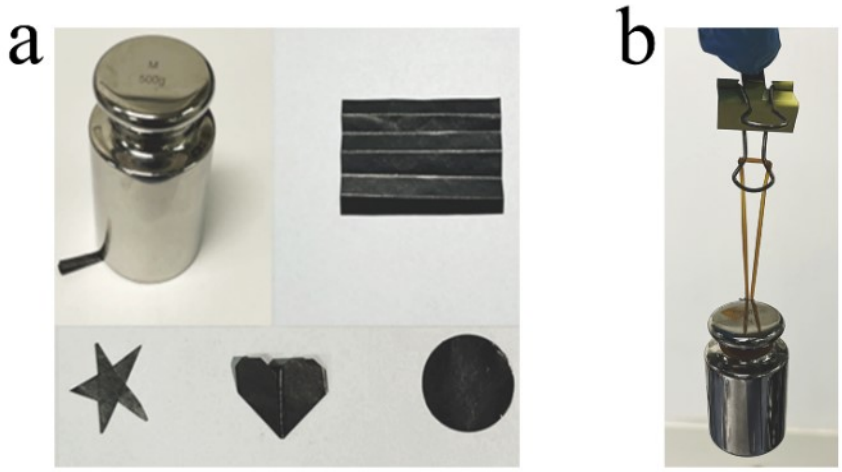

Fig. S27 (a) Optical images demonstrating the flexibility, bending resistance, and ease of shaping of the annealed composite film. (b) Mechanical robustness of the annealed composite film, evidenced by a 3.6 mg sample lifting a 200 g weight.

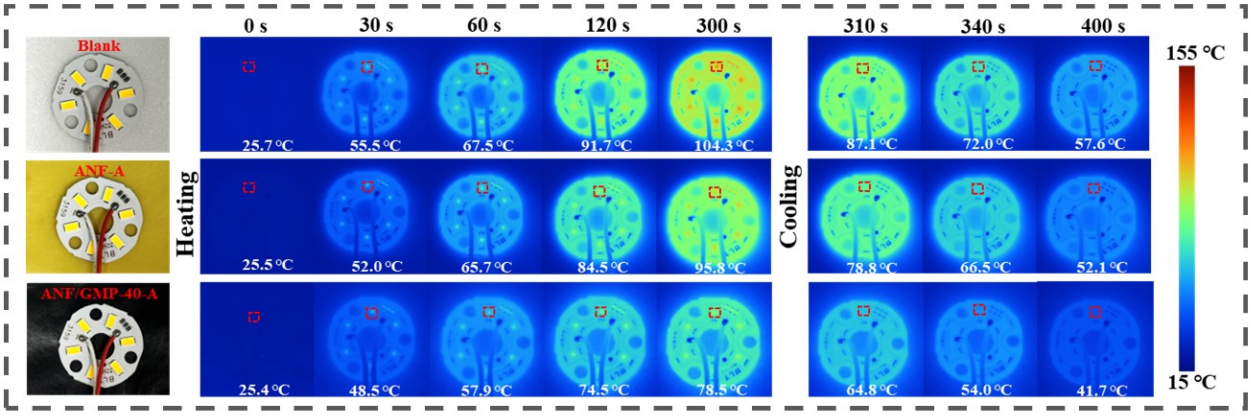

Fig. S28 Infrared thermal images showing the temperature distribution when using the annealed ANF and ANF/GMP composite films as the heat dissipation component for the thermal management of LED.

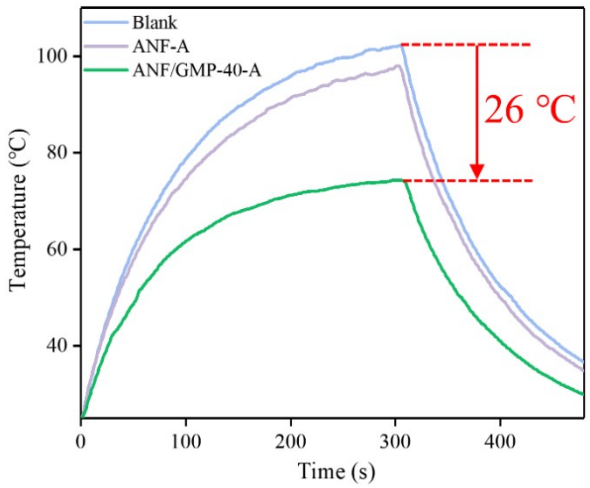

Fig. S29 Surface temperature-time curves of LED when using the annealed ANF and ANF/GMP composite films as the heat dissipation component.

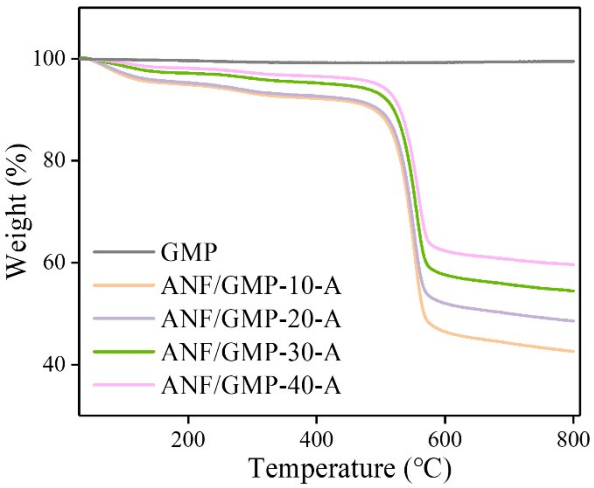

Fig. S30 TGA curves of the annealed ANF/GMP composite films.

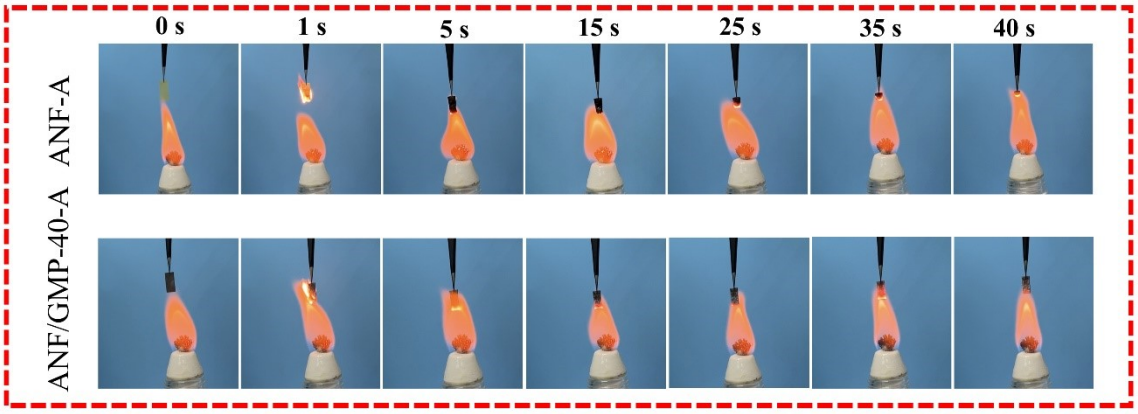

Fig. S31 Snapshots of vertical combustion tests for the annealed ANF and ANF/GMP films.

3. Supplementary Tables

Table S1 Atomic ratios of C, O and N in ANF films.

Sample	C (%)	O (%)	N (%)
ANF	77.84	5.89	16.27
ANF-200	81.29	4.50	14.21
ANF-300	80.96	3.90	15.14

Table S2 Binding energies and contents of C-C, C-N and C=O in C1s XPS bands.

Sample	C-C		C-N		C=O		π-π interaction	
	Binding energy (eV)	Content (%)	Binding energy (eV)	Content (%)	Binding energy (eV)	Content (%)	Binding energy (eV)	Content (%)
ANF	284.80	70.01	285.88	12.80	287.94	7.21	288.75	9.98
ANF-200	284.78	64.78	285.50	21.82	288.01	7.42	291.00	5.99
ANF-300	284.77	67.32	285.59	20.23	287.99	7.54	291.63	4.91

Table S3 A comparison of the thermal conductivity of ANF/GMP-30-A and ANF/GMP-40-A composite films with the previously-reported thermally conductive composite films.

Filler	Matrix	Content of fillers (wt%)	Thermal conductivity (W m^{-1} K^{-1})	Elongation at break (%)	Tensile strength (MPa)	Refs.
GNP	ANF	50	30.42	~33.5	304.1	S3
Graphene	ANF	40	48.20	18.6	~170.0	S4
GNP	CNF	40	21.42	~5.6	115.8	S5
Graphene	ANF	30	6.00	2.75	~175.0	S6
GS	CNF	10	6.75	\	84.5	S7
rGO	NFC	1	12.60	1.5	107.0	S8
GMP	ANF	50	64.00	~6.0	~105.0	S9
BNNS	ANF	30	46.70	5.6	~165.0	S10
LM@GN	ANF	32.5	5.67	3.7	20.0	S11
IL@BNNS	ANF	40	15.20	22.3	63.2	S12
s-IL@BNNS	ANF	40	23.00	24.5	129.0	S13
BNNS	CNF	50	17.30	~7.5	125.0	S14
Mxene	NFC	30	22.43	1.7	71.4	S15
Mxene	ANF	30	15.50	14.3	52.7	S16
GF	CNF	40	48.20	\	188.5	S17
GMP	**ANF**	**30**	**58.36**	**6.0**	**179.5**	**This work**
		40	**68.06**	**6.1**	**165.0**	

*GNP: graphene nanoplatelet, rGO: reduced graphene oxide, GS: graphene sheets, BNNS: boron nitride nanosheet, *m*-BN: benzidine-functionalized boron nitride, s-IL@BNNS: imidazolium cationic functionalized ILs-modified BNNSs, CNF: cellulose nanofiber, GMP: Graphite microplatelets, NFC: nanofibrillated cellulose, GF: Carbon fiber.

References

S1 H. Sun, S.J. Mumby, J. R. Maple, A. T. Hagler, *J. Am. Chem. Soc.*, 1994, **116**, 2978–2987.

S2 S. Plimpton, *J. Comput. Phys.*, 1995, **117**, 1–19.

S3 Z. Luo, P. Han, B. Yu, W. Yan, X. Chen, Y. Feng, H. Zheng, H. Guo, Z. Cheng and J. He, *Carbon*, 2024, **226**, 119142.

S4 L. Huang, G. Xiao, Y. Wang, H. Li, Y. Zhou, L. Jiang and J. Wang, *Nano-Micro Lett.*, 2022, **14**, 168.

S5 B. Zhang, L. Wang, C. Zhang and S. Wu, *Chem. Eng. J.*, 2022, **439**, 135675.

S6 T. T. V. Tran, V.-A. Le, C.-H. Nguyen, D.-V. N. Vo, T. M. Nguyen, C. Samart, S. Kongparakul, S. Ghotekar and C. M. Vu, *ACS Appl. Nano Mater.*, 2022, **5**, 12991–13001.

S7 N. Song, S. Cui, D. Jiao, X. Hou, P. Ding and L. Shi, *Carbon*, 2017, **115**, 338–346.

S8 N. Song, Q. Wang, D. Jiao, H. Pan, L. Shi and P. Ding, *Compos Part A-Appl S*, 2021, **143**, 106261.

S9 Y.-Y. Song, N. Jiang, S.-Z. Li, L.-N. Wang, L. Bai, J. Yang and W. Yang, *Mater. Horiz.*, 2025, **12**, 4260–4273.

S10 K. Wu, J. Wang, D. Liu, C. Lei, D. Liu, W. Lei and Q. Fu, *Adv. Mater*, 2020, **32**, e1906939.

S11 W. Luo, B. Wei, T. Luo, B. Li and G. Zhu, *Small*, 2024, **20**, 2406574.

S12 X. Li, B. Wu, Y. Lv, R. Xia and J. Qian, *J. Mater. Chem. A*, 2024, **12**, 864–875.

S13 X. Li, B. Wu, Y. Lv, R. Xia and J. Qian, *Chem. Eng. J.*, 2025, **503**, 158246.

S14 X. Wan, X. Xia, Y. Chen, D. Lin, Y. Zhou and R. Xiong, *Polymers*, 2024, **16**, 805.

S15 E. Jiao, K. Wu, Y. Liu, M. Lu, H. Zhang, H. Zheng, C. Xu, J. Shi and M. Lu, *Compos Part A-Appl S*, 2021, **143**, 106290.

S16 Y. Zhan, X. Zheng, B. Nan, M. Lu, J. Shi and K. Wu, *Eur. Polym. J.*, 2023, **186**, 111847.

S17 M. C. Vu, D. Mani, T.-H. Jeong, J.-B. Kim, C.-S. Lim, H. Kang, M. A. Islam, O.-C. Lee, P. J. Park and S.-R. Kim, *Chem. Eng. J.*, 2022, **429**, 132182.